# Mapping Nutrients Content in a Nematode-Infected Coffee Plantation by Empirical Models Derived from RapidEye Image

## Mapeamento do Conteúdo de Nutrientes da Cultura Cafeeira Infectada por Nematoides por Meio de Modelos Empíricos Derivados de Imagens do RapidEye

George Deroco Martins[1]; Maria de Lourdes Bueno Trindade Galo[2];
Bruno Sérgio Vieira[1]; Ricardo Falqueto Jorge[3] & Cinara Xavier de Almeida[3]

[1]*Universidade Federal de Uberlândia – UFU/ Programa de Pós Graduação em Agricultura e Informações Geoespaciais.*
*Rod. LMG 746, km 01, s/n, bloco 1, Campus Monte Carmelo. CEP: 38500-000. Monte Carmelo, MG, Brasil*
[2] *Universidade Estadual Paulista - UNESP/ Programa de Pós Graduação em Ciências Cartográficas.*
*Rua Roberto Simonsen, 305. Bairro: Centro  Caixa Postal 468 - 19060-900 – Presidente Prudente - SP, Brasil*
[3]*Universidade Federal de Uberlândia – UFU/ Instituto de Ciências Agrárias, Campus Monte Carmelo.*
*Rod. LMG 746, km 01, s/n, bloco 1, Campus Monte Carmelo. CEP: 38500-000. Monte Carmelo, MG, Brasil*
*E-mails: deroco@ufu.br; trindade.galo@unesp.br; brunovieira@ufu.br; falqueto@ufu.br; cinara@ufu.br*

**Resumo**

Os nematoides estão entre os mais importantes patógenos do café, causando perdas significativas de produtividade. A infecção do cafeeiro por nematoides pode comprometer o sistema radicular, induzindo a manifestação de sintomas reflexos na parte superior da planta. Além do mais, as deficiências nutricionais podem desencadear um aumento na predisposição do hospedeiro a vários outros patógenos. Assim, o monitoramento dos níveis nutricionais de plantas cultivadas em áreas predispostas à ocorrência de nematoides é fundamental. Neste estudo, foi avaliado o potencial de modelos empíricos para estimar os teores de macro e micronutrientes em uma área experimental de café infestada por nematoides, a partir de uma imagem multiespectral RapidEye. Para isso, análises laboratoriais foram realizadas para determinar as concentrações de macro e micronutrientes, bem como do nível de infestação por nematoides, em duas parcelas experimentais instaladas na região cafeeira de Monte Carmelo (MG). Verificou--se que a correlação entre teor de nutrientes e concentração de nematoides no solo foi maior para Mg, S, Cu e Mn (coeficientes de correlação igual a 0,62, 0,51, 0,71 e 0,75, respectivamente), enquanto outros nutrientes como o Ca tiveram correlações mais altas com as bandas espectrais ou índices de vegetação superiores a 0,7, com todos os índices derivados das bandas espectrais de vermelho, vermelho distante e infravermelho próximo. Os modelos empíricos para a estimativa dos nutrientes foram produzidos a partir das bandas espectrais e índices de vegetação com correlações maiores que 0,5. A banda do vermelho limítrofe, posicionada em uma região espectral sensível a variações na vegetação, participou individualmente dos modelos para inferir as concentrações dos macronutrientes Mg e S e dos micronutrientes B, Cu, Fe e Mn, porém todos resultaram em coeficientes de calibração inferiores a 0,41. A banda do infravermelho próximo foi usada na estimativa dos teores de N, P e Na, com R2 igual a 0,25, 0,36 e 0,49, respectivamente. O NDVI participou da formulação do modelo de inferência do teor de Ca e resultou no maior R2 de calibração (0,61), embora o erro de validação tenha sido alto (13,56%). Os mapas coropléticos da distribuição espacial de Ca, Mg, Cu, Fe, Mn e Zn apresentaram uma configuração similar, evidenciando concentrações elevadas e quase homogêneas desses nutrientes em quase toda a área experimental. Os teores de Na e B foram diferentes nas duas parcelas que compõem a área experimental, enquanto K e S tiveram uma distribuição mais heterogênea. Os mapas de N e P refletem bem a deficiência desses nutrientes na totalidade da área, principalmente no conteúdo de P. Os modelos empíricos ajustados para a estimativa da maioria dos nutrientes foram consistentes com a condição de excesso ou deficiência nutricional na área experimental. Palavras chave: estimativa do teor de nutrientes; nematoides na cultura cafeeira; imagem multispectral RapidEye

**Palavras chave:** estimativa do teor de nutrientes; nematoides na cultura cafeeira; imagem multispectral RapidEye

**Abstract**

Nematodes are among the most important coffee pathogens, causing significant losses of productivity. The infection of the coffee plant by nematodes can compromise the root system inducing the manifestation of reflex symptoms in its upper part. In addition, nutritional deficiencies may trigger an increase in host predisposition to various other pathogens. Thus, the monitoring of the nutritional levels of plants grown in areas predisposed to the occurrence of nematodes is fundamental. In this study, it was evaluated the potential of empirical models to estimate macro and micronutrient contents in an coffe experimental nematode infested area from a RapidEye multispectral image. For this purpose, laboratory analyzes were performed to determine the contents of macro and micronutrients, as well as the level of nematode infestation, in two experimental plots located in the coffee region of Monte Carmelo (MG). It was verified that the correlation between nutrient content and nematode concentration was higher for the Mg, S, Cu and Mn (correlation coefficients of 0.62, 0.51, 0.71 and 0.75, respectively), while other nutrients had higher correlations with spectral bands or vegetation indices, mainly Ca which had coefficients higher than 0.7 with all indices derived from the spectral bands of red, red edge and near infrared. Empirical models for nutrient estimation were generated from spectral bands and vegetation indices with correlations greater than 0.5. The red edge band, positioned in a spectral region sensitive to variations in vegetation, individually participated in the models to infer the concentrations of the macronutrients Mg and S, besides the micronutrients B, Cu, Fe and Mn, but all calibrated with correlation coefficients below 0,41. The near infrared band was used in the estimation of the N, P and Na contents (R2 equal to 0.25, 0.36 and 0.49, respectively). The NDVI participated in the formulation of the inference model of Ca content and resulted in the highest calibration R2 (0.61), although the validation error was high (13.56%). The choropleth maps of Ca, Mg, Cu, Fe, Mn and Zn spatial distribution had a similar configuration, indicating almost homogeneous and high concentrations of these nutrients in most of the experimental area. The Na and B contents were different in the two plots of the experimental area, while K and S had a more heterogeneous distribution. The maps of N and P reflect well the deficiency of these nutrients in the whole area, mainly in the P content. The empirical models adjusted for the estimation of most of the nutrients were consistent with the condition of excess or deficiency of nutrients in the experimental area.

**Keywords:** nutrient content estimation; nematodes in the coffee crop; multispectral image RapidEye

## 1 Introduction

Coffee (*Coffea* spp.) is the most valuable agricultural commodity in international trade. Brazil is the largest producer of this commodity that generates profits and support millions of direct and indirect jobs for many people who participate in the production chain from planting to the commercialization of the final product.

The productivity currently obtained in commercial crops is far below the potential, since it is neither possible nor economically viable to remove all factors limiting the development of crops, such as the supply of nutrients in adequate concentrations and balanced relations (Malavolta *et al*., 1997), competition with weeds and mainly damages caused by insect pests and pathogens (Povh *et al*., 2008). In addition, the expansion of cropping areas in nutrient-deficient soils, greater nutrient removal due to increased productivity and the inadequate incorporation of limestone or its use in high concentrations, have accelerated the emergence of problems related to nutritional deficiencies in the plants.

Phytonematodes are among the most important coffee pathogens, causing significant loss of productivity in several species, mainly *C. arabica* and *C. robusta* (Barros *et al*., 2014; Jones *et al*., 2013). The infection of coffee plants by pathogens as root nematodes of *Meloidogyne* and *Pratylenchus* genera can compromise the root system inducing the manifestation of reflex symptoms in the upper part of the plant in the same way as the nutritional deficiencies (Jones *et al*., 2013) which, in turn, can trigger an increase in the predisposition of the host to several pathogens by reducing tolerance or resistance, including nematodes. Thus, the implementation of measures such as phytosanitary control, post-harvest care, adequate fertilization management program and the selection of cultivars with suitable agronomic characteristics, contribute to a satisfactory production of coffee plantations (Galdeano *et al*., 2010).

In recent decades, remote sensing has become an important decision-making tool in the crop management process and a number of new spaceborne multispectral sensors with narrow and appropriate spectral bands are in operation. Some have a chlorophyll-sensitive red edge band at about 710 nm that has been shown to provide accurate information on the subtle variations in the structure and vegetation condition (Cho *et al*., 2012). Hence, the images generated by multispectral sensors embedded in orbital platforms, such as the RapidEye system, have enabled the detection and mapping of agricultural crops infected by pathogens, pests or insects (Martins & Galo, 2014; Martins *et al*., 2017) and the detection of foliar nutrient content by multispectral indices (Eitel *et al*., 2011).

In agriculture, most empirical models and vegetation indices derived from multispectral images have the purpose of mapping agricultural crops, estimating biophysical parameters, such as biomass, leaf area index and chlorophyll (Feilhauer & Martin, 2015; Jay *et al*., 2016; Zarco Tejada *et al*., 2013), to develop physiological studies (Casas *et al*., 2015) and discriminating plant diseases (Apan *et al*., 2004; Ashourloo *et al* 2016; Belasque Jr. *et al*., 2008; Cho *et al*., 2012; Hillnhünter *et al*., 2011; Huang *et al*., 2012; Hunt Jr. *et al*., 2013; Lins *et al*., 2009; Mahlein *et al*., 2013; Marcassa *et al*., 2006; Martins & Galo, 2014; Oumar *et al*., 2013). The models used in estimating nutrient content are based on the relation between the spectral response of vegetation in specific spectral bands or vegetation indices, with foliar nutrient content (Hernandez-Clemente *et al*., 2017; Pellissier *et al*., 2015).

Considering that the phytonematodes occurrence in the soil causes a nutritional breakdown in the plant, samples of coffee leaves and soil were collected and laboratory analyzes were performed in an experimental area of coffee infected with nematodes, in order to evaluate the correlation between the nematodes concentration and the macro and micronutrients contents. In addition, given the spectral configuration of some orbital systems that include a red-edge band, the aim of this study was to evaluate the potential of empirical models generated from specific spectral bands and vegetation indices derived from a RapidEye image in estimating the macro and micronutrients contents in this experimental area located in Monte Carlo municipality, Minas Gerais State.

## 2 Material and Methods
### 2.1 Experimental Area and Field data

The experiment was performed in a coffee plantation located in Minas Gerais State, in Monte Carmelo municipality (UTM coordinates centered in 230300 E, 7929400 N / 23S, Reference System WGS 84), in a experimental area of 14 hectares. The soil type is dystrophic Red Latosol and the area has been cultivated with *Coffea arabica* L. (Arabica coffee) for thirteen years. The last renovation of this cultivated field occurred in February 2012 with a planting configuration of 3.8 meters between rows and spacing of 0.7 meters between plants.

The sampled plot is characterized by the phytonematodes incidence with plants presenting pathogen-induced reflex symptoms (plant defoliation) but without the presence of the specific pattern of small clearings along the planting rows, associated with agricultural crops installed in areas infected by nematodes. Because it is an experimental area destined to different agronomic studies, the late symptoms of infection by nematodes are not evident, since the plants are submitted to constant treatments, such as fertilization and application of nematicides. Nutrients and nematological concentrations were estimated from the material collected in a single field campaign on March 10, 2015. The sampling points were defined in 60 stations configured in a regular grid with a size of 50 x 50 m (Figure 1). At each sampling station a coffee plant was considered and 100 leaves per plant were collected in the region of the plant's basal third. The position of the points was obtained from a relative geodetic survey with a pair of Topcon Hiper L1 / L2 GNSS receivers.

Laboratory analysis of leaf tissue was performed to determine the nutritional levels of the plants. The evaluated macronutrients were: nitrogen (N), phosphorus (P), potassium (K), calcium (Ca), magnesium (Mg), sulfur (S) and sodium (Na), and the micronutrients were: boron (B), copper (Cu), iron (Fe), manganese (Mn) and zinc (Zn).

The nematological analysis was preceded by the soil extraction in the sugar flotation method, according to Jenkins *et al*. (1964). Then, the identification of the genus of the nematode and the microscopic count of the number of individuals per cm³ were made. In this study, the nematode concentration was estimated by the number of juveniles per 150 cm³. But, by convention, we will refer to this measure as the concentration of nematodes per cm³.

### 2.2 Multispectral Image Processing

In order to correlate the radiometric properties of the multispectral image with the nutrient contents, a RapidEye image was obtained from the satellite
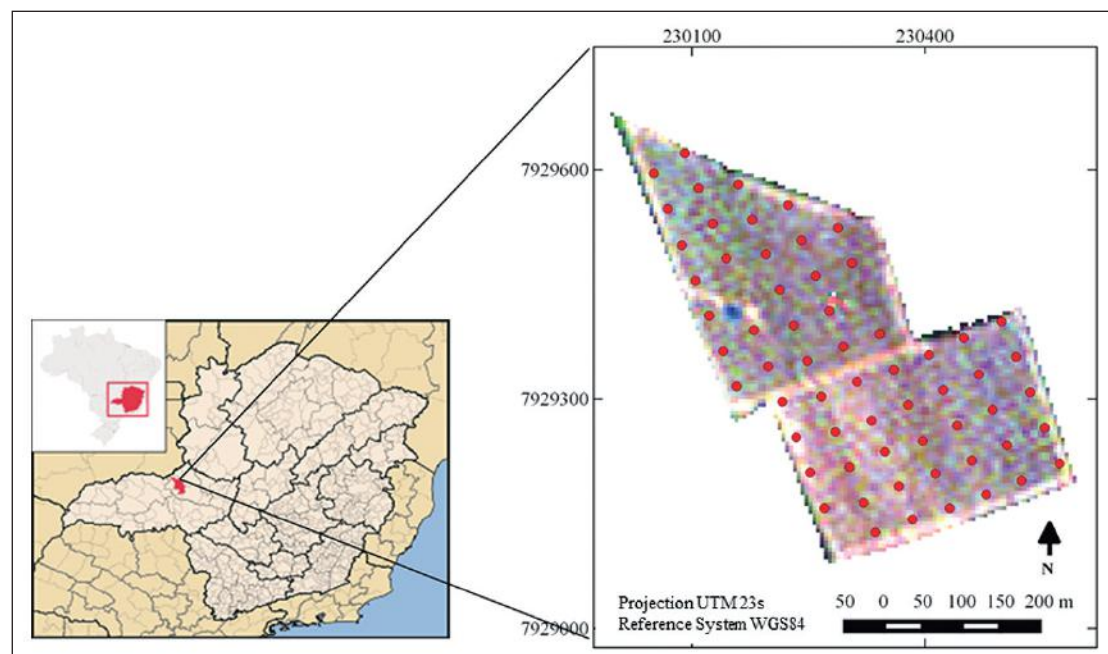


Figure 1 Location of the experimental area and configuration of soil and leaves sampling stations. The circles in red represent the points sampled (60 stations)

image catalog of the Ministry of the Environment, accessible to Brazilian Public institutions (http://geocatalogo.mma.gov.br). The RapidEye image was taken on December 12, 2014, almost 4 months prior to the field campaign, a period of time that can be significant when correlating field data with image. However, in this period of time there was no agricultural management in this experimental area (with a nematode infection), and because it is a perennial crop, it can be considered that the coffee tree maintains its nutritional components practically unchanged in the absence of agricultural management (Barros *et al*., 2014).Although the RapidEye system sensor has the GSD (Ground Sample Distance) of 6.5 meters in the nadir acquisition, the Ministry of the Environment provides orthorectified images with a pixel size of 5 meters and a global spatial accuracy of 10 meters. So, the image was obtained with processing level Basic 1B, which includes geometric correction and radiometric calibration. On the other hand, the atmospheric correction was required because the RapidEye image did not include treatment to minimize the effects of atmospheric absorption and electromagnetic radiation scattering. This correction was performed using the Fast Line-of-sight Atmospheric Analysis of Hypercubes (FLAASH) correction method, implemented in the Environment for Visualizing Images (ENVI) software. FLAASH is based on MODerate resolution atmosphere TRANsmittance (MODTRAN4) code, which requires the prior definition of the aerosol model, geographic location, elevation, satellite altitude, date and time of acquisition, and other atmospheric parameters (such as the $CO_2$ concentration). Some of the parameters required by FLAASH were extracted from the RapidEye image metadata file. The concentration of water vapor was derived from

the MOD07-L2 MODIS/Terra product, whose acquisition was coincident with the image. The specification of the aerosol model (tropical) and other variables followed the recommendations of Felde *et al*. (2003) and Adler-Golden *et al*. (1999). As in Houborg *et al*. (2017) it was necessary to use a scale factor of 1000 on the image pixels in the atmospheric correction process, so that the reflectance value of the pixels which have attributes expressed in surface reflectance were positive.

## 2.3 Definition of Vegetation Indices and Empirical Models

Among the spectral bands and vegetation indices evaluated for the generation of the models, the five original bands of the RapidEye sensor were considered: blue band – 1 (centered at 475 nm), green band – 2 (centered at 555 nm), red band – 3 (centered at 657.5 nm), red edge band – 4 (centered at 710 nm) and near infrared band – 5 (centered at 810 nm). The vegetation indices evaluated were: the classical NDVI (Normalized Difference Vegetation Index), resulting from the use of near infrared and red bands; $NDVI_{3,4}$, defined by the normalized difference between the red edge (4) and the red (3) bands; $NDVI_{4,5}$, normalized difference between edge red (4) and near infrared (5); an index derived from the red edge by near infrared bands ratio, named VOGRE (Vogelmann Red Edge) (Vogelmann *et al*., 1993); the Carotenoid Reflectance Index – CIR (Gitelson *et al*., 2002); the Structure Insensitive Pigment Index – SIPI (Penuelas *et al*., 1995); and Enhanced Vegetation Index – EVI (Huete *et al*., 1997). The indices are defined according to the equations showed in Table 1.

| Index | Description | Fórmula | Reference |
|---|---|---|---|
| NDVI | Normalized Difference Vegetation Index | $(R_{805} - R_{657.5}) / (R_{805} + R_{657.5})$ | Rouse *et al*., 1994 |
| $NDVI_{3,4}$ | Red-Edge and Red Normalized Difference | $(R_{710} - R_{657.5}) / (R_{710} + R_{657.5})$ | Gitelson & Merzluak, 1994 |
| $NDVI_{4,5}$ | NIR and Red-Edge Normalized Difference | $(R_{805} - R_{710}) / (R_{805} + R_{710})$ | Gitelson & Merzluak, 1994 |
| VOGRE | Vogelmann Red Edge | $R_{710} / R_{805}$ | Vogelmann *et al*., 1993 |
| CRI | Carotenoid Reflectance Index | $(1 / R_{555}) / (1 / R_{710})$ | Gitelson *et al*., 2002 |
| SIPI | Structure Insensitive Pigment Index | $(R_{805} - R_{475}) / (R_{805} + R_{710})$ | Penuelas *et al*., 1995 |
| EVI | Enhanced Vegetation Index | $2.5(R_{805} - R_{657.5}) / (R_{805} + 6R_{657.5} - 7.5R_{475} + 1)$ | Huete *et al*., 1997 |

Table 1 Vegetation indices derived from RapidEye spectral bands investigated in this study. R refers to surface reflectance, NIR is the near infrared band and the subscript numbers in the formulas are the central wavelengths of the spectral band considered in nm.

In the specification of models to estimate the nutrient content only those spectral bands and vegetation indices that defined correlation coefficients greater than 0.5 were considered, for a p-value less than 0.05. Although no guidance was found in the literature, a correlation greater than 50% was adopted to ensure that the predictors of the models were somehow related to the variable being inferred (nutrient content).

The empirical models were defined from simple and multiple linear regression equations between the radiometric values (corrected for surface reflectance) extracted from the RapidEye image and the nutrient levels of the leaves obtained in the chemical analysis. For the definition of the models, 40 sample elements from the original sample of 60 elements (Figure 1) were randomly specified.

In the validation of the empirical models we considered the 20 sample elements of the total sample, not used in the definition of the models. From the discrepancies between the macro and micronutrient contents estimated by the models and the concentrations obtained in the laboratory analysis of the leaves collected in the 20 validation points, the error analyses were performed using the root mean squared error (RMSE, equation 1) and the root mean squared error percent (%RMSE, equation 2) to verify the residual.

$$\text{RMSE} = \sqrt{\frac{\sum_{i=1}^{n}(x_i - x_{med})^2}{n}} \qquad (1)$$

$$\%\text{RMSE} = \sqrt{\frac{\sum_{i=1}^{n}(x_i - x_{med})^2}{n}} \, X \, \frac{100Xn}{\sum_{i=1}^{n} x_{med}} \qquad (2)$$

where $x_i$ and $x_{med}$ represent the concentrations estimated by the model and the nutrient contents determined in the laboratory analysis respectively, and n is the number of sample points.

Finally, empirical models were used to generate Choropleth maps of the concentration of macro and micronutrients. In these maps, the values resulting from the application of the specific models were classified into three ranges of foliar levels of nutrients, according to the reference values defined in Ribeiro *et al*. (1999). Values that are within the thresholds specified (shown in the last column of Table 2) by the authors indicate the estimated concentrations that are in the optimal range of each nutrient, values lower than the lower limit point to concentrations below the sufficiency range, and values above the specified upper limit indicate nutrient super concentration.

## 3 Results and Discussions
## 3.1 Foliar Nutrients Content

Table 2 shows the descriptive statistics (average, standard deviation, minimum and maximum values) of the macro and micronutrients contents determined in the laboratory analysis of the leaves collected *in situ*, considering the complete sample (60 sample points) and the reference values which specify low, ideal and high levels of nutritional levels of leaves, according to Ribeiro *et al*. (1999).

Comparing the values of the averages indicated in Table 2 with the reference values established

| Nutrient | | Mean | SD | Min | Max | Reference* |
|---|---|---|---|---|---|---|
| Macro (g kg⁻¹) | N | 25.311 | 1.942 | 21.0 | 29.6 | 27 < N g·kg⁻¹ < 32 |
| | P | 1.053 | 0.131 | 0.7 | 1.5 | 1.5 < P g·kg⁻¹ < 2 |
| | K | 12.941 | 2.161 | 7.4 | 19.3 | 19 < K g·kg⁻¹ < 24 |
| | Ca | 14.772 | 2.171 | 8.7 | 18.8 | 10 < Ca g·kg⁻¹ < 14 |
| | Mg | 3.785 | 0.798 | 2.3 | 6.3 | 3.1 < Mg g·kg⁻¹ < 3.6 |
| | S | 1.745 | 0.101 | 1.4 | 2.0 | 1.5 < S g.kg⁻¹ < 2 |
| | Na | 0.827 | 0.066 | 0.8 | 1.0 | 1.9 < Na g·kg⁻¹ < 1.95 |
| Micro (mg kg⁻¹) | B | 63.582 | 11.191 | 34.98 | 92.27 | 59 < B mg·kg⁻¹ < 80 |
| | Cu | 11.993 | 6.552 | 3.98 | 44.78 | 8 < Cu mg·kg⁻¹ < 16 |
| | Fe | 156.882 | 20.142 | 118.29 | 213.54 | 90 < Fe mg·kg⁻¹ < 180 |
| | Mn | 171.597 | 34.645 | 108.06 | 278.69 | 120 < Mn mg·kg⁻¹ < 210 |
| | Zn | 23.462 | 7.151 | 10.73 | 42.70 | 8 < Zn mg·kg⁻¹ < 16 |

Table 2 Descriptive statistics of the coffee leaf nutrients content (macro and micronutrients) and reference values based on Ribeiro *et al*., 1999. Statistics metrics used were: average (Mean), standard deviation (SD), minimum value (Min) and maximum value (Max) in g·kg⁻¹ for macronutrients and mg·kg⁻¹ for micronutrients. * Reference values defined by Ribeiro et at (1999) indicating the range of sufficiency of each nutrient.

in Ribeiro *et al.* (1999), the main macronutrients N, P, K and Na present values below the recommended concentration, while Ca, Mg (macronutrient) and Zn (micronutrient) have concentrations higher than the reference values. The other nutrients S, B, Cu, Fe and Mn show values within the range considered as normal nutrition.

## 3.2 Correlations Between Nutrients Content and Nematodes Concentration

From the nematological analysis, five genera of nematodes were found in the study area: *Meloidogyne, Pratylenchus, Criconemella, Helicotylenchus* and *Paratylenchus*. Migratory endoparasite nematodes such as those of the *Pratylenchus* genus cause direct damage or lesions in the roots of the plants, while sedentary nematodes as those of the *Meloidogyne* genus infect internally the roots and form giant cells that function as specialized feeding sites. This difference has direct implications for the water absorption and, consequently, of nutrients. Migratory nematodes also have direct action in reducing the absorption of water and nutrients since they cause a decrease of the root surface until the destruction of the roots. In the sedentary nematodes there is the compromise of root growth without direct destruction of the root tissues. Although in different ways and intensities, both migratory and sedentary genera compromise the absorption of water and nutrients.

Considering the above, we consider the total concentration of phytonematodes, without distinction of genus, to evaluate their correlation with the contents of the different macro and miconutrients. In the graph shown in Figure 2, the correlation coefficients obtained between the contents of each of the macronutrients (N, P, K, Ca, Mg, S, Na) and micronutrients (B, Cu, Fe, Mn and Zn) and the concentration of total phytonematodes in 150 $cm^3$ of soil are indicated.

Among the macronutrients, Mg and S presented the higher positive correlation coefficients with the concentration of total phytonematodes in 150 $cm^3$ of soil (0.62 and 0.51, respectively). Although the micronutrients Mn and Cu resulted in correlation coefficients higher than 0.7 all of them indicate a positive association between the nematodes concentration and the levels of these nutrients, whose measurements were within the reference levels (Table 2) in leaves samples collected *in situ*.

Regarding the interaction between Arabica coffee and nematodes of the species *Meloidogyne exigua*, the results described in the literature concerning the effect of the pathogen on the absorption and translocation of nutrients are sometimes contradictory. Macedo *et al.* (1974) found no changes in N, P, Ca, K, Mg, Cu, Fe and Mn in the leaves of coffee inoculated with the pathogen. Santos *et al.* (1981) reported a reduction in Ca and N contents



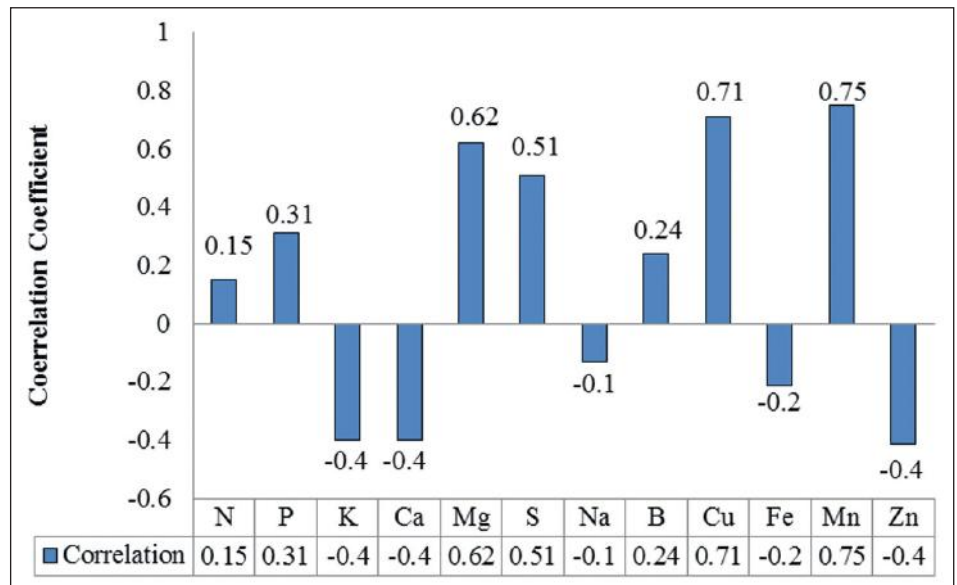| | N | P | K | Ca | Mg | S | Na | B | Cu | Fe | Mn | Zn |
|---|---|---|---|---|---|---|---|---|---|---|---|---|
| ■ Correlation | 0.15 | 0.31 | -0.4 | -0.4 | 0.62 | 0.51 | -0.1 | 0.24 | 0.71 | -0.2 | 0.75 | -0.4 |

Figure 2 Correlation coefficient between coffee leaf nutrients and total phytonematode concentration in 150 cm³ of soil.

and unchanged levels of P, K and Mg, not observing the accumulation of any of these nutrients in the roots of the inoculated coffee plants. Boneti *et al*. (1982) found lower absorption of Zn, Cu, Fe, Mn and B in inoculated coffee plants, while Gonçalves *et al*. (1998) reported that leaves of coffee inoculated with the pathogen did not show changes in N, Ca and Cu contents, but a decrease in P, Mg, Fe, Mn and B contents and increase in K and Zn levels. In this study, we did not identify an explicit association between the different levels of nematodes infection with the macronutrients that presented lower levels than those recommended in Ribeiro *et al*. (1999), as occurred in the experimental area with N, P, K and Na concentrations.

## 3.3 Correlations Between Nutrients Content and Spectral Data

The correlation coefficients presented in the Figure 3 graphs indicate the relationships between the surface reflectance values of the spectral bands centered at 475 (blue), 555 (green), 657.5 (red), 710 (red edge) and 805 (near infrared) nm, as well as the vegetation indices derived from the RapidEye image (NDVI, $NDVI_{3,4}$, $NDVI_{4,5}$, VOGRE, SIPI and EVI) with the nutrient contents analyzed. Figure 3a refers to the macronutrients (N, P, K, Ca, Mg, S and Na) and Figure 3b to the micronutrients (B, Cu, Fe, Mn and Zn).



| A | R475 | R555 | R657,5 | R710 | R805 | NDVI | NDVI3,4 | NDVI4,5 | VOGRE | SIPI | EVI |
|---|---|---|---|---|---|---|---|---|---|---|---|
| Na | -0.138 | -0.114 | -0.173 | -0.045 | 0.621 | 0.343 | 0.409 | 0.24 | 0.436 | -0.289 | 0.319 |
| S | -0.063 | -0.211 | -0.421 | -0.566 | 0.181 | 0.375 | 0.413 | 0.294 | 0.419 | -0.37 | 0.433 |
| Mg | -0.224 | -0.239 | -0.399 | -0.464 | 0.075 | 0.317 | 0.297 | 0.263 | 0.253 | -0.377 | 0.263 |
| Ca | -0.534 | -0.495 | -0.726 | -0.577 | 0.678 | 0.775 | 0.744 | 0.707 | 0.717 | -0.767 | 0.683 |
| K | 0.323 | 0.379 | 0.525 | 0.43 | -0.437 | -0.538 | -0.51 | -0.475 | -0.478 | 0.585 | -0.473 |
| P | 0.143 | 0.247 | 0.135 | -0.023 | -0.513 | -0.283 | -0.311 | -0.237 | -0.332 | 0.244 | -0.273 |
| N | 0.293 | 0.262 | 0.371 | 0.266 | -0.619 | -0.495 | -0.534 | -0.403 | -0.546 | 0.442 | -0.474 |

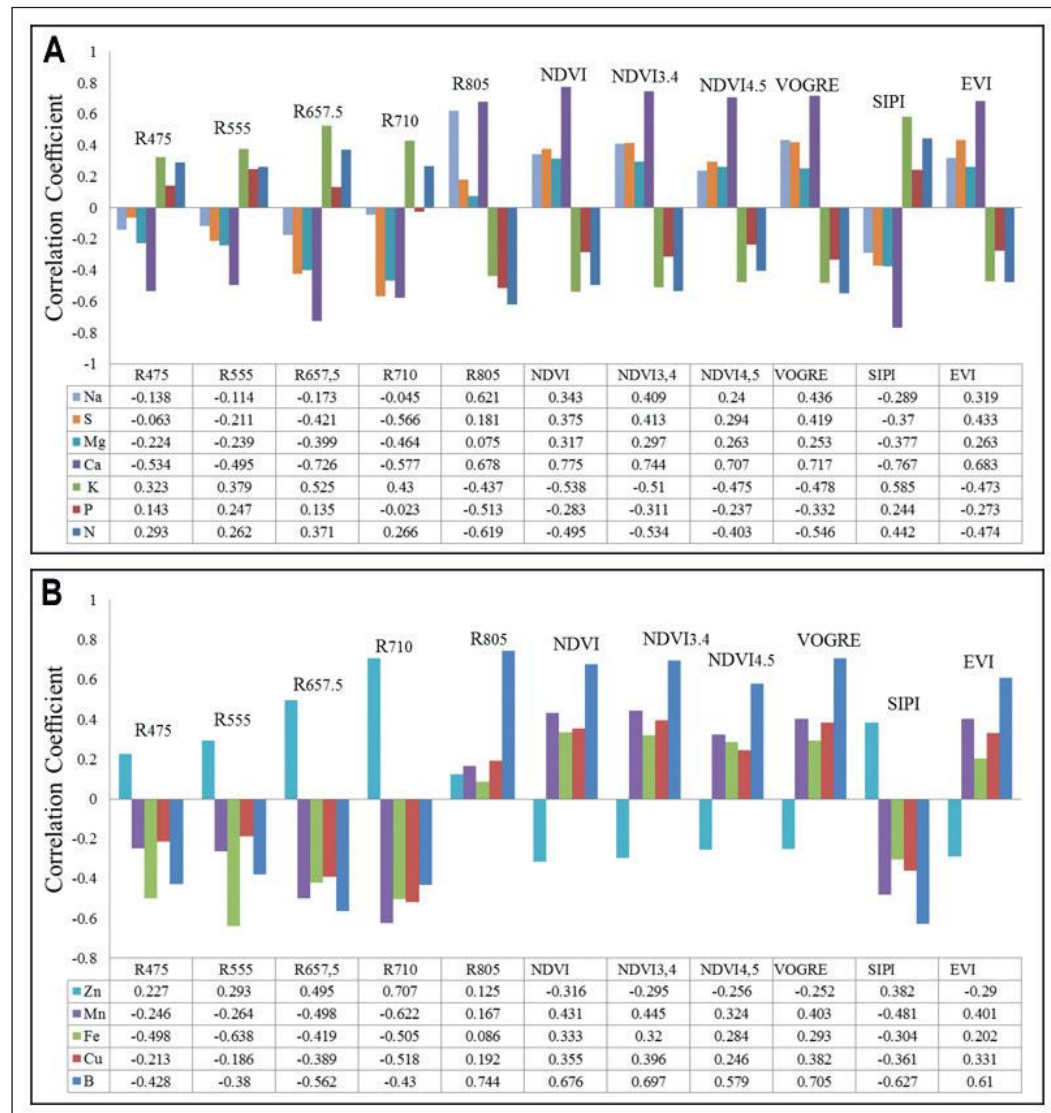| B | R475 | R555 | R657,5 | R710 | R805 | NDVI | NDVI3,4 | NDVI4,5 | VOGRE | SIPI | EVI |
|---|---|---|---|---|---|---|---|---|---|---|---|
| Zn | 0.227 | 0.293 | 0.495 | 0.707 | 0.125 | -0.316 | -0.295 | -0.256 | -0.252 | 0.382 | -0.29 |
| Mn | -0.246 | -0.264 | -0.498 | -0.622 | 0.167 | 0.431 | 0.445 | 0.324 | 0.403 | -0.481 | 0.401 |
| Fe | -0.498 | -0.638 | -0.419 | -0.505 | 0.086 | 0.333 | 0.32 | 0.284 | 0.293 | -0.304 | 0.202 |
| Cu | -0.213 | -0.186 | -0.389 | -0.518 | 0.192 | 0.355 | 0.396 | 0.246 | 0.382 | -0.361 | 0.331 |
| B | -0.428 | -0.38 | -0.562 | -0.43 | 0.744 | 0.676 | 0.697 | 0.579 | 0.705 | -0.627 | 0.61 |

Figure 3 Correlation coefficients between the surface reflectance and vegetation indices derived from RapidEye multispectral image and macro (a) and micronutrients (b)

In the graphs, the correlations defined by the variables that resulted in correlation coefficients higher than 0.5 or lower than -0.5 meet the level of significance of 95% (p-value <0.05). Figure 3a indicates that the correlation coefficients between the macronutrients and the visible spectral bands were less expressive than those obtained with the near infrared band ($R_{805}$) and the vegetation indices. The correlations for the blue ($R_{475}$), green ($R_{555}$), red ($R_{657.5}$) and red edge ($R_{710}$) bands do not meet the level of significance of 95% (p-value <0.05), with the exception of correlations between K and $R_{657.5}$ band (0.525), S and $R_{710}$ band (-0.566) and Ca with the $R_{475}$, $R_{657.5}$ and $R_{710}$ spectral bands (-0.534, -0.726 and -0.577, respectively).

Among the original spectral bands, the near infrared ($R_{805}$) showed a higher correlation with at least four macronutrients: N, P, Ca and Na (-0.619, -0.513, 0.678 and 0.621, respectively). In this wavelength range, this can be attributed to the greater sensitivity of the vegetation to nutritional variations in the leaves, as well as to a better discrimination between healthy vegetation and those nematode-infected, as reported in Usha *et al*. (2013).

The vegetation indices showed a higher correlation with three macronutrients: Ca, K and N. Ca was correlated with all indices, defining the lowest value for the EVI (0.683) and the highest correlation with the SIPI, reaching -0.767. K presented a significant correlation with NDVI (-0.538), $NDVI_{3.4}$ (-0.510) and SIPI (0.585) indices and N was correlated with $NDVI_{3.4}$ (-0.534) and VOGRE (-0.546).

The only macronutrient that defined an average concentration above the reference was Mg (Table 2), although its content showed a lower correlation with any of the spectral indicators evaluated (band or vegetation index). However, the Ca levels showed high correlation with all the original bands and vegetation indices (with a single exception in the $R_{555}$ band) and this higher correlation registered with the vegetation index SIPI (-0.767).

Regarding macronutrient contents determined in the nematode-infected experimental area that were below the recommended average levels (N, P and K, Table 2), only K defined a higher correlation, with

a visible spectrum band centered on $R_{657.5}$ (0.525). However, this relationship, as with Ca (0.726), may also be associated with the chlorotic state in senescent leaves or necrosis in leaf margins, since severe stress on vegetation caused by foliar dehydration, for example, usually manifests itself in this spectral range (Thenkabail *et al*., 2012).

Evaluating leaf N levels in corn and wheat cereals, Pohv *et al*. (2008) found correlations higher than 0.9 with NDVI. But in this study, the correlation coefficients obtained between N and K contents in coffee leaves and the normalized vegetation indexes were negative and did not exceed the value of -0.54. Particularly in relation to the N content, the highest correlation obtained was -0.619, with spectral band $R_{805}$.

The correlation coefficient between the micronutrients and the original RapidEye bands were higher than the correlations with the vegetation indices (Figure 3b). The $R_{710}$ spectral band showed a high correlation for three micronutrients: Cu, -0.518, Mn, -0.622 and Zn, 0.707, and the bands $R_{555}$ and $R_{805}$ presented the highest correlation for Fe (-0.638) and B (0.744).

The significant correlations of Zn, Mn, Fe and Cu with the band centered in $R_{710}$ and the B with $R_{805}$ is due to the association of these micronutrients to the photosynthetic process and, therefore, to the plant chloroplasts, responsible for the spectral characteristics of the effects of absorption and scattering present in the range of 600 to 800 nm (Jensen, 2008). The symptoms of the deficiency of these nutrients are characterized by the chlorosis of the leaves, making the pigments sensitive to the electromagnetic radiation of the red edge (Thenkabail *et al*., 2012). The B was the only micronutrient that correlated with vegetation indices with values higher than 0.57.

## 3.4 Accuracies of the Empirical Models for Nutrients Content Estimation

Most of the empirical models were generated from simple regression, with the exception of the equations defined for the estimation of the nutrients P, Na and Zn, as shown in Table 3. The red edge band

($R_{710}$ centered range) was the spectral band that was present in the largest number of empirical models, it was present in the estimation of five nutrients: Mg, S, B, Mn and Zn. Another frequent spectral range in the models was the near infrared ($R_{805}$), contributing in the estimation of N, P and Na.

In addition to suitable indicators for nutrient estimation, such as N, near-infrared and red-edge spectral bands (Lepine *et al.*, 2016) have been found to be appropriate for crop discrimination and insect detection (Oumar and Mutanga, 2013; Adelabu *et al.*, 2014), nematodes (Martins and Galo, 2014) and other pathogens (Usha *et al.*, 2003).

The NDVI, a spectral index classically used to detect vegetation stress, integrated the empirical model for estimating Ca ($R^2$(calibration) = 0.61, $R^2$(validation)=0.33, RMSE = 2.08 and %RMSE = 13.56%). The vegetation index derived from the ratio of the red-edge and red reflectance ($NDVI_{3,4}$), composing with the band centered on $R_{710}$, presented good performance in predicting the Zn content ($R^2$(calibration) = 0.60, $R^2$(validation) = 0.45, RMSE =

2.84 and %RMSE = 17.52). The EVI, VOGRE and SIPI, included in the models for estimation of Na, P and K, respectively, resulted in determination coefficients below 0.5.

The spectral band centered on $R_{710}$ (red-edge) was the only variable included in the adjusted models for the estimation of the macronutrients Mg and S and the micronutrients B, Cu, Fe and Mn, all with determination coefficient less than 0.42. The empirical model for estimation of Fe content defined a calibration $R^2$ equal to 0.41, but had the highest validation errors ($R^2$=0.15, RMSE=73.26 and %RMSE=45.57%).

Previous studies have already demonstrated the possibility of estimating the plant nutrient content from empirical models derived from data acquired by sensors embedded in orbital platforms. Nutter *et al.* (2002) evaluated the protein concentration in a nematode-infected soybean crop by means of an empirical model derived from the near infrared spectral band of the ETM+/Landsat 7 system, with a calibration $R^2$ of 0.90. In studies using images with

| Nutrient | | Empirical Model | $R^2$ (calibration) | $R^2$ (validation) | RMSE (validation) | %RMSE (validation) |
|---|---|---|---|---|---|---|
| Macro | N | 34.5 - 30.7· $R_{805}$ | 0.27 | 0.13 | 2.08 | 8.3 |
| | P | 2.14 - 2.61· $R_{805}$ - 0.162·VOGRE | 0.36 | 0.10 | 0.15 | 14.75 |
| | K | -1.23 + 10·SIPI | 0.35 | 0.40 | 1.82 | 14.18 |
| | Ca | 2.51 + 21.4·NDVI | 0.61 | 0.33 | 2.08 | 13.56 |
| | Mg | 9.22 - 39.5· $R_{710}$ | 0.22 | 0.15 | 0.73 | 19.93 |
| | S | 2.62 - 6.38· $R_{710}$ | 0.32 | 0.24 | 0.08 | 4.72 |
| | Na | 0.095 + 3.08· $R_{805}$ - 0.254·EVI | 0.49 | 0.34 | 0.18 | 22.56 |
| Micro | B | - 46,2 + 0.035· $R_{710}$ | 0.19 | 0.10 | 8.84 | 13.37 |
| | Cu | 45,6 - 242· $R_{710}$ | 0.17 | 0.14 | 3.26 | 19.20 |
| | Fe | 238,4 - 153· $R_{710}$ | 0.41 | 0.15 | 73.26 | 45.57 |
| | Mn | 433 - 1818· $R_{710}$ | 0.40 | 0.33 | 32.02 | 18.36 |
| | Zn | - 134 + 895· $R_{710}$ + 91.3·$NDVI_{3,4}$ | 0.60 | 0.45 | 2.84 | 17.52 |

Table 3 Empirical models for the macro and micronutrients estimation. $R^2$ is the coefficient of determination of the models calibration and RMSE and %RMSE are the validation errors.

less spatial detailing (30 m), the correlations of empirical models were even higher, as in Noori *et al*. (2016) that obtained coefficients of determination of 0.98 and 0.99 in the estimation of B and K contents, respectively, from a model that included the SAVI (Soil Adjusted Vegetation Index) derived from ALOS AVNIR 2 images with spatial resolution of 10 m.

In a recent study to evaluate the performance of the Sentinel-2 MSI spectral bands and vegetation indices in the empirical estimate of N in coffee leaf, Chemura *et al*. (2018) obtained calibration $R^2$ values between 0.24 and 0.57 for the spectral bands and

from 0.28 to 0.66 using the vegetation indeces most related to the N content. The authors also report that the combination of optimized bands and vegetation indices (by means of random forest variable optimization) produced better results in the modeling of N content in coffee ($R^2 = 0.78$).

The validation data allowed expressing the relationship between the measured (x-axis) and predicted (y-axis) macro and micronutrient levels in the coffee leaves, as presented in the plots of Figure 4. The performance of each model is also presented through the Root Mean Square Error (RMSE) and percent error.
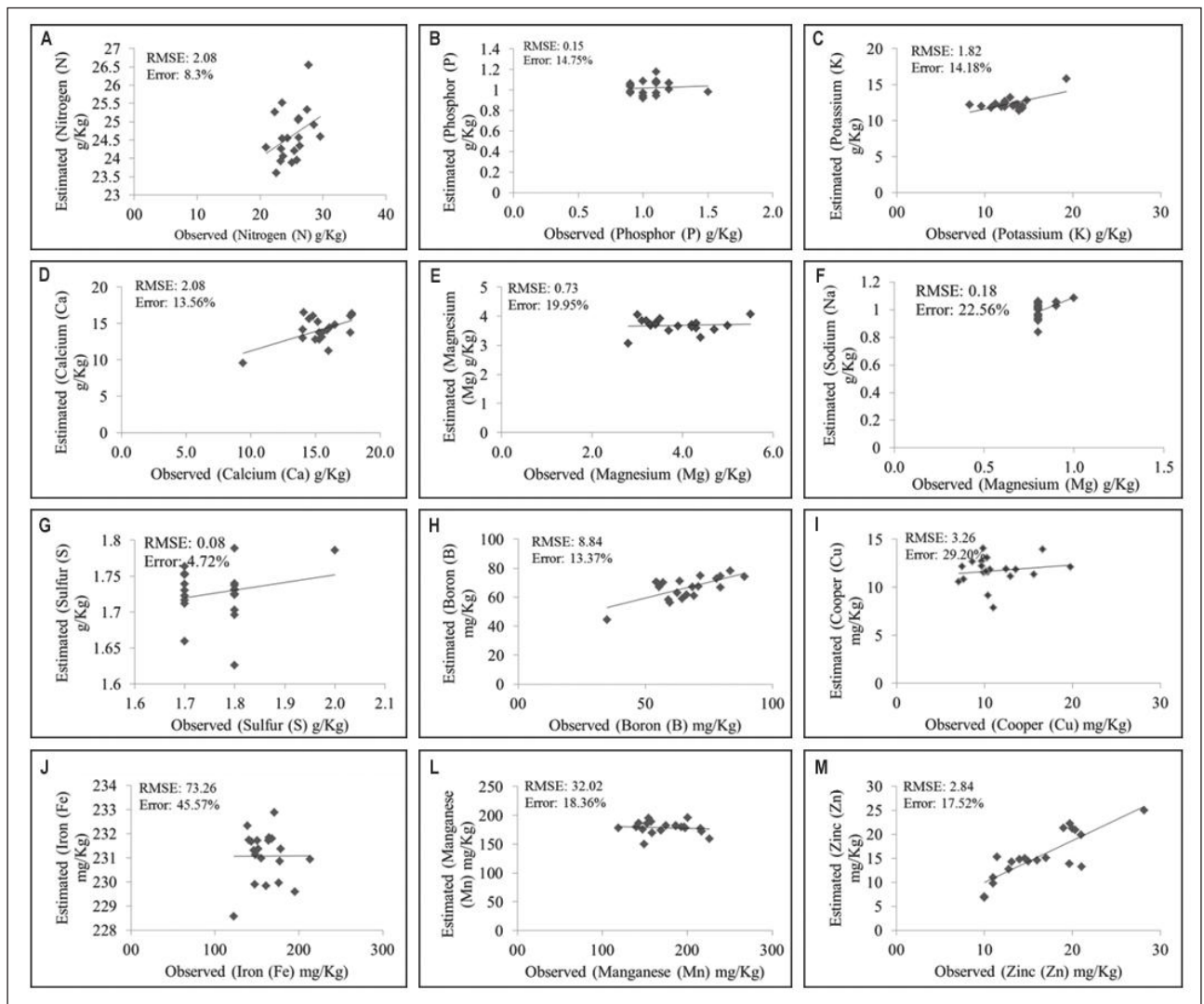


Figure 4 Plots showing the relationship between measured (x-axis) and predicted (y-axis) coffee foliar macronutrients (A) N, (B) P, (C) K, (D) Ca, (E) Mg, (F) S, (G) Na and micronutrient (H) B, (I) Cu, (J) Fe, (K) Mn and (L) Zn levels

Among the macronutrients, the empirical models that presented better performance expressed by the smallest error of estimation were S (4.72%) and Ca (8.3%). The largest errors were recorded in the estimate of Na (22.56%) and Mg (19.93%). In Oumar *et al*. (2014), the macronutrient deficiency in eucalyptus was estimated with a maximum error of 3.7%, based on empirical models derived from the red edge band of an image taken by the WorldView 2 system, which has greater geometric detail (GSD = 2.4 m) compared with the RapidEye image. Considering the micronutrients, the empirical models that presented the smallest error of estimation were those of B (13.37%) and Fe (17.52%). The highest errors were reported in the estimation of Mn (18.36%), Cu (19.20%) and Fe (45.57%).

## 3.5 Spatial Distribution of the Nutrients Content in Experimental Area

Figure 5 shows the Choropleth maps of the nutrient contents generated from empirical models for the two plots of the experimental area. The specification of the low, normal and high concentration ranges (associated to very light brown, light brown and dark brown, respectively, in the maps) was based on Ribeiro *et al*. (1999). The N, P, K, Ca, Mg, S and Na macronutrients are showed in the maps of Figures 5a to 5g, while the micronutrients B, Cu, Fe, Mn and Zn are expressed in maps of Figures 5h to 5l, respectively.

The spatial dispersion maps of the macronutrient contents indicate that the concentration of N in the experimental area (Figure 5A) remained at the ideal levels in the lower plot, but significant areas of the upper plot showed N deficiency. However, the greatest nutritional deficiencies were observed for P and K. The P content (Figure 5B) was below the recommendation of Ribeiro *et al*. (1999) for coffee trees in practically the entire experimental area. For the concentration of K (Figure 5C), the areas within the ideal range were spread along the two plots.

On the other hand, the mapping of Ca and Mg levels indicated the predominance of high concentrations of these macronutrients, and only specific parts of the two experimental plots presented Ca and Mg contents above the levels considered adequate

for coffee. For Ca (Figure 5D), areas with less than ideal concentration occurred in the upper plot, while for Mg (Figure 5E) a narrow strip of nutritional deficiency was observed on the left in both plots, but this deficiency was also verified in a second broader strip, in the lower part of the experimental area. The dispersion of the S content (Figure 5F) showed a similar variability in the two plots of the experimental area, with predominance of medium and high concentrations. However, in the map indicating the Na dispersion (Figure 5F) deficiency of this nutrient in the lower plot was observed, maintaining medium to high concentrations in the upper plot.

The spatial configuration of micronutrient occurrence also showed variations among them, as in the case of macronutrients. The B content (Figure 5H) had a similar spatial dispersion as that of the macronutrient Na, with a concentration within the values recommended in the lower plot, but with a predominance of zones of high concentrations of B in the upper plot. Above-average nutrient levels predominated in the maps generated for the Cu (Figure 5I) and Mn (Figure 5K), which presented strips of lower concentration on the left of the experimental area, mainly in the lower plot. Predominance of high concentrations occurred also for Fe and Zn. However, while the Fe content (Figure 5J) defined small areas with medium and low concentrations of this nutrient mainly to the left of the experimental area, for the Zn content (Figure 5L) ideal values were observed in small dispersed areas in the upper plot and areas concentrated on strips located to the right on the lower plot.

## 4 Conclusions

This study was carried out in an area of coffee infected with nematodes in order to evaluate the potential of empirical models to estimate macro and micronutrient contents from a multispectral image RapidEye and showed the feasibility of this estimation for several nutrients with different degrees of accuracy.

In the exploratory analysis of the data it was verified that, while the micronutrients defined concentrations at or above the reference levels, import-
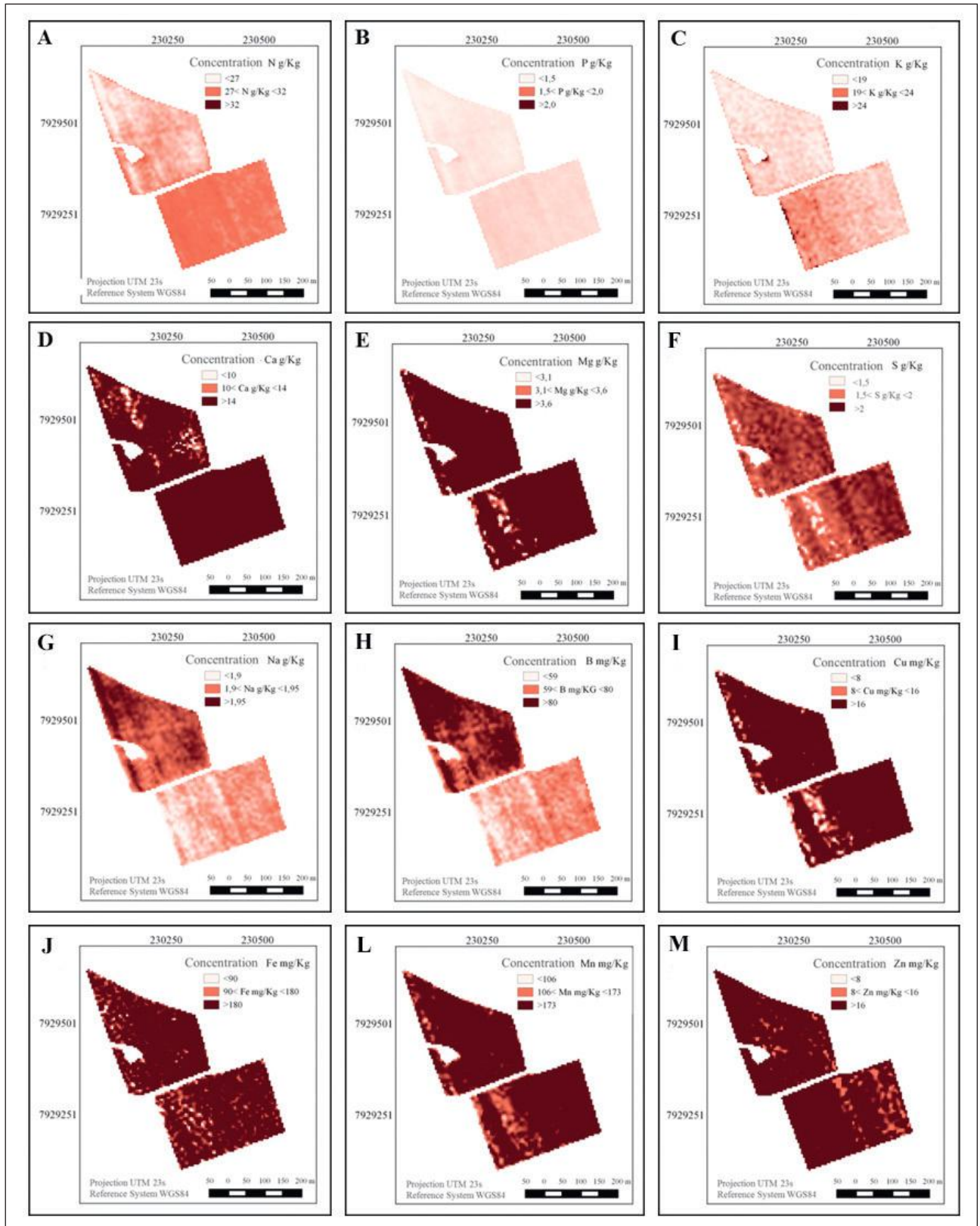
Figure 5 Choropleth maps representing the macronutrients contents in g·kg⁻¹: (A) N, (B) P; (C) K; (D) C; (E) Mg; (F) S and (G) Na, and micronutrients levels in mg·kg⁻¹: (H) B; (I) Cu; (J) Fe; (K) Mn and (L) Zn. The legend colors indicate the concentration ranges defined in Ribeiro *et al*. (1999) as low (very light brown), medium (light brown) and high (dark brown).

ant macronutrients, such as N, P, K and Na, presented concentrations below the values specified by Ribeiro *et al*. (1999). On the other hand, although the experimental area is characterized by a marked occurrence of nematodes, only the Mg and S macronutrients and the Cu and Mn micronutrients had a significant correlation with the nematode concentration. The absence of a pattern in the relationship between deficits in the concentration of some nutrients and the higher levels of infection by the pathogen is recurrently reported in the literature.

The highest correlations between the nutrient contents in the coffee and the spectral data derived from the RapidEye image were obtained for the original bands of the red edge (centered in $R_{710}$) and near infrared ($R_{805}$). The classical NDVI vegetation index showed a highest correlation with the Ca content ($R^2$ = 0.775).

The maps indicating the spatial distribution of Ca, Mg, Cu, Fe, Mn and Zn presented a similar configuration, evidencing high and almost homogeneous concentrations of these nutrients in almost the entire experimental area. The mapping of Na and B contents indicated different concentrations of these nutrients for the two plots that compose the experimental area, while for K and S, this distribution was more heterogeneous. The N and P maps reflect well the deficiency of these nutrients in the totality of the area experienced, mainly in the content of P. Thus, although the correlations between the nutrient content of some of the analyzed nutrients and the level of nematode infection were low and sometimes contradictory, the empirical models adjusted for the estimation of most of the nutrients were consistent with their condition of excessive or deficient concentration in the experimental area.

On the other hand, the mapping of the spatial distribution of nutrient concentrations along the plots of an agricultural crop is a crucial issue in Precision Agriculture, one of the pillars of sustainable agricultural production. In this sense, spatial inference through empirical models and from multispectral images allow the representation of the spatial heterogeneity of crop needs for the entire field, in a more agile and cost-effective way.

## 6 References

Adelabu, S.; Mutanga, O & Adam, E. 2014. Evaluating the impact of red-edge band from RapidEye image for classifying insect defoliation levels. *ISPRS Journal of Photogrammetry and Remote Sensing*, *95*: 34-41.

Adler-Golden, S. M.; Matthew, M. W.; Bernstein, L. S.; Levine, R. Y.; Berk, A.; Richtsmeier, S. C.; Prabhat, K. A.; Anderson, G. P.; Jerry, W. F.; Gardner, J. A.; Hoke, M. L.; Jeong, L. S.; Pukall, B. P.; Ratkowski, A. J. & Hsiao-hua, K. Burke. 1999. Atmospheric correction for shortwave spectral imagery based on MODTRAN4. *In*: SPIE'S INTERNATIONAL SYMPOSIUM ON OPTICAL SCIENCE, ENGINEERING, AND INSTRUMENTATION, Denver, CO, United States, 1999, p. 1-9.

Apan, A.; Held, A.; Phinn, S. & Markley, J. 2004. Detection of sugarcane 'orange rust' disease using EO-1 Hyperion hyperspectal imagery. *International Journal of Remote Sensing*, *25*: 489–498.

Ashourloo, D.A.; Matkan, A.; Huete, A.; Aghighi, H. & Mobasheri, M.R. 2016. Developing an Index for Detection and Identification of Disease Stages. IEEE Geoscience and Remote Sensing Letters, *13*(6): 851-855.

Barros, A.F.; Oliveira, R.D.L.; Lima, I.M.; Coutinho, R.R.; Ferreira, A.O. & Costa, A. 2014. Root-knot nematodes, a growing problem for Conilon coffee in Espírito Santo state, Brazil. *Crop Protection*, *55*(1): 74-79.

Belasque Junior, J.; Gasparoto, M.C.G. & Marcassa, L. G. 2008. Detection of mechanical and disease stresses in citrus plants by fluorescence spectroscopy. *Appl. Opt*. *47*(11): 1922-1926.

Boneti, J. I. S., Ferraz, S., Braga, J. M., Oliveira, L. M. (1982). Influência do parasitismo de Meloidogyne exigua sobre a absorção de micronutrientes (Zn, Cu, Fe, Mn e B) e sobre o vigor das mudas de cafeeiro. Fitopatologia Brasileira, *1*(7): 197-207.

Casas, A.; Riaño, D.; Ustin, S. L.; Dennison, P. & Salas, J. 2014. Estimation of water-related biochemical and biophysical vegetation properties using multitemporal airborne hyperspectral data and its comparison to MODIS spectral response. *Remote Sensing of Environment*, *148*(1): 28-41.

Chemura, A.; Mutanga, O.; Odindi, J. & Kutywayo, D. 2018. Mapping spatial variability of foliar nitrogen in coffee (*Coffea arabica L*.) plantations with multispectral Sentinel-2 MSI data. *ISPRS Journal of Photogrammetry and Remote Sensing*, *138*(1):1–11.

Cho, M.A.; Debba, P.; Mutanga, O.; Dudeni-Tlhone, N.; Magadla, T. & Khuluse, A.S.; Potential utility of the spectral red-edge region of SumbandilaSat imagery for assessing indigenous forest structure and health. *International Journal Of Applied Earth Observation And Geoinformation*, *116*(1): 85-93.

Eitel, J.U.H.; Vierling, L.A.; Litvak, M.E.; Long, D.S.; Schulthess, U.; Ager, A. A.; Krofcheck, D.J. & Stoscheck, L. 2011. Broadband, red-edge information from satellites improves early stress detection in a New Mexico conifer woodland. *Remote Sensing of Environment*, *115*(12): 3640–3646.

Feilhauer, H.; Asner, G.P. & Martin, R.E. 2015. Multi-method ensemble selection of spectral bands related to leaf biochemistry. *Remote Sensing Of Environment*, **164**(1): 57-65.

Felde, G.W.; Anderson, G.P.P.; Adler-Golden, S.M.; Matthew, N.W. & Berk, A. 2003. Analysis of Hyperion data with the FLAASH atmospheric correction algorithm. *In*: PROCEEDINGS. INTIERNATIONAL GEOSCIENCE. REMOTE SENSING SYMPOSIUM, 2003. Toulouse, France, p. 90–92.

Galdeano, D.M.; Guzzo, S.D.; Patricio, F.R.A. & Ricardo, H. 2010. Proteção do cafeeiro contra cercosporiose por Acibenzolar-S-Metil e proteína harpina. *Pesquisa Agropecuária Brasileira*, **45**(1): 686-692.

Garrity, S.R.; Allen, C.D.; Brumby, P.B.; Gangodagamage, C. MacDowell, N.G. & Cai, D.M. 2013. Quantifying tree mortality in a mixed species woodland using multitemporal high spatial resolution satellite imagery. Remote Sensing of Environment, **129**(1): 54–65.

Gitelson, A. & Merzlyak, M. 1994. Spectral Reflectance Changes Associated with Autumn Senescence of *Aesculus Hippocastanum L.* and *Acer Platanoides L.* Leaves. *Journal of Plant Physiology*, **143**(1): 286292.

Gonçalves, W.; Silvarolla, M.B. & Lima, M.M.A. 1998. Estratégias visando à implementação do manejo integrado dos nematoides parasitos do cafeeiro. *Informe Agropecuário*, **1**(19): 36-47.

Hernández-Clemente, R.; North, P.R.J.; Hornero, A. & Zarco-Tejada, P.J. 2017. Assessing the effects of forest health on sun-induced chlorophyll fluorescence using the FluorFLIGHT 3-D radiative transfer model to account for forest structure. *Remote Sensing Of Environment*, **193**(1): 165-179.

Hillnhütter, A.C.; Mahlein, K.; Sikora, R. A. & Oerke, E. C. 2011. Remote sensing to detect plant stress induced by Heterodera schachtii and Rhizoctonia solani in sugar beet fields. *Field Crops Research*, **122**(1): 70-77.

Houborg, R. & Mccabe, M. F. 2017. Impacts of dust aerosol and adjacency effects on the accuracy of Landsat 8 and RapidEye surface reflectances. *Remote Sensing Of Environment*, **194**(1): 127-145.

Jianrong, H.; Liao, H.; Yubo, Z.; Sun, J.; Sun, Q. & Liu, X. 2012. Hyperspectral detection of rice damaged by rice leaf folder (Cnaphalocrocis medinalis). *Computers and Electronics in Agriculture*, **82**(1): 100–107.

Raymond, E. H.; Doraiswamy, P. C.; McMurtrey, J. E.; Daughtry, C. S. T.; Perry, E. M. & Akhmedov, B. 2013. A visible band index for remote sensing leaf chlorophyll content at the canopy scale. *International Journal of Applied Earth Observation and Geoinformation*, **21**(1): 103-112.

Jay, S.; Bendoula, R.; Hadoux, X.; Féret, J. B. & Gorretta, N. 2016. A physically-based model for retrieving foliar biochemistry and leaf orientation using close-range imaging spectroscopy. *Remote Sensing of Environment*, **177**(1): 220-236.

Jenkins, W.R. 1964. A rapid centrifugal-flotation technique for separating nematodes from soil. *Plant Disease Reporter, 48(1): 692-695.*

Jones, J.T.; Haegeman, A.; Danchin, E.G.; Gaur, H.S.; Helder, J.; Jones M.G.; Kikuchi, T.; Manzanilla-López, R.; Palomares-Rius, J.E.; Wesemael, W.M. & Perry, R.N. 2013. Top 10 plant-parasitic nematodes in molecular plant pathology. *Molecular Plant Pathology*, **14**(9): 946-961.

Lepine, L.C.; Ollinger, V.S.; Ouimette, A.P. & Martin, M. E. 2016. Examining spectral reflectance features related to foliar nitrogen in forests: Implications for broad-scale nitrogen mapping. *Remote Sensing of Environment*, **173**(1): 174-186.

Lins, E.C.; Belasque, J. & Marcassa, L.G. 2009. Detection of citrus canker in citrus plants using laser induced fluorescence spectroscopy. *Precision Agric*, **10**(4): 319-330.

Macedo, M.C.M.; Haag, H.P. & Lordello, L.G.E. 1974. Influencia do nematoide Meloidogyne exigua Goeldi, 1887, na absorção de nutrientes em plantas jovens de cafeeiro. *Nematologia Brasileira*, **1**(1): 54-72.

Mahlein, A.K.; Rumpf, T.; Welke, P.; Dehne, H. W.; Plümer, L.; Steiner, U & Oerke., E.C. 2013. Development of spectral indices for detecting and identifying plant diseases. *Remote Sensing of Environment*, **128**(1): 21-30.

Marcassa, L.G.; Gasparoto, M.C.G. & Belasque, J. 2006. Fluorescence spectroscopy applied to orange trees. *Laser Physics*, **16**(5): 884-888.

Martins, G.D. & Galo, M.L.B.T. Detecção de áreas infestadas por nematoides e Migdolus fryanus em cultura canavieira a partir de imagens multiespectrais Rapideye. 2014. *Revista Brasileira de Cartografia*, Brasília, **2**(66): 285-301

Martins, G.D.; Galo, M.L.B.T. & Vieira, B.S. 2017. Detecting and Mapping Root-Knot Nematode Infection in Coffee Crop using Remote Sensing Measurements. IEEE *Journal of Selected Topics in Applied Earth Observations and Remote Sensing, 10*(12): 5395-5403.

Noori, O. & Panda, S. S. 2016. Site-specific management of common olive: Remote sensing, geospatial, and advanced image processing applications. *Computers And Electronics In Agriculture*, **127**(1): 680-689.

Oumar, Z.; Mutanga, O. & Ismail, R. 2013. Predicting Thaumastocoris peregrinus damage using narrow band normalized indices and hyperspectral indices using field spectra resampled to the Hyperion sensor. *International Journal Of Applied Earth Observation And Geoinformation*, **21**(1): 113-121.

Oumar, Z. & Mutanga, O. 2014. Integrating environmental variables and WorldView-2 image data to improve the prediction and mapping of Thaumastocoris peregrinus (bronze bug) damage in plantation forests. *Isprs Journal Of Photogrammetry And Remote Sensing*, **87**(1): 39-46.

Pellissier, P.A.; Ollinger, S.V.; Lepine, L.C.; Palace, M.W. & McDowell, W.H. 2015. Remote sensing of foliar nitrogen in cultivated grasslands of human dominated landscapes. *Remote Sensing of Environment*, **167**(1): 88-97.

Povh, F.P.; Molin, J.P.; Gimenez, L.M.; Pauletti, V.; Molin, R. & Salvi, J.V. 2008. Comportamento do NDVI obtido por sensor ótico ativo em cereais. *Pesquisa Agropecuária Brasileira*, **43** (8): 1075-1083.

Ribeiro, R.C.F.; Ferraz, S.; Mizobutsi, E.H. & Mendes, M. 1999. Levantamento de espécies de Monacrosporium predadoras de nematoides em diversas regiões brasileiras. *Nematologia Brasileira*, **23**(2):41-47.

Santos, J. M.; Ferraz, S. & Oliveira, L.M. 1981. Efeitos do parasitismo de Meloidogyne exigua sobre a absorção e translocação de nutrientes em mudas de cafeeiro. *Fitopatologia Brasileira*, **1**(6): 333-340.

Usha, K. & Singh, B. 2013. Potential applications of remote sensing in horticulture-A review. *Scientia Horticulturae*, **153**(1): 71-83.

Zarco-Tejada, P.J.; Catalina, A.; González, M.R. & Martín, P. Relationships between net photosynthesis and steady-state chlorophyll fluorescence retrieved from airborne hyperspectral imagery. *Remote Sensing of Environment*, **136**(1): 247-258.